Transaction B: Mechanical Engineering
Vol. 17, No. 1, pp. 61–74
© Sharif University of Technology, February 2010

SCIENTIA
IRANICA

Maximum Allowable Dynamic Load of Flexible Manipulators Undergoing Large Deformation

M.H. Korayem[1,*], **M. Haghpanahi**[1] **and H.R. Heidari**[1]

Abstract. *In this paper, a general formula for finding the Maximum Allowable Dynamic Load (MADL) of geometrically nonlinear flexible link manipulators is presented. The dynamic model for links in most mechanisms is often based on the small deflection theory but for applications like light-weight links, high-precision elements or high speed it is necessary to capture the deflection caused by nonlinear terms. First, the equations of motion are derived, taking into account the nonlinear strain-displacement relationship using Finite Element Method (FEM) approaches. The maximum allowable loads that can be achieved by a mobile manipulator during a given trajectory are limited by a number of factors. Therefore, a method for determination of the dynamic load carrying capacity for a given trajectory is explained, subject to the accuracy, actuator and amplitude of residual vibration constraints and by imposing a maximum stress limitation as a new constraint. In order to verify the effectiveness of the presented algorithm, two simulation studies considering a flexible two-link planar manipulator mounted on a mobile base are presented and the results are discussed. The simulation results indicate that the effect of introducing geometric elastic nonlinearities and inertia nonlinearities on the maximum allowable loads of a manipulator.*

Keywords: *Flexible link; Finite element; Large deformation; Load; Residual vibration.*

INTRODUCTION

The dynamic analysis of high speed mechanisms, space robot arms and flexible structures has received considerable attention in the past two decades. Most of the researchers, however, assume small deformation and use a linear strain displacement relationship. When accurate mathematical models are required, nonlinear elastic deformation in structures may have to be considered. Nonlinearities can arise out of nonlinear elastic, plastic and viscoelastic behavior, or there can be geometric nonlinearities arising out of large deformations.

A high payload to mass ratio is one of the advantages of flexible robot manipulators. In traditional manipulators, the maximum allowable dynamic load is usually defined as the maximum load that a manipulator can repeatedly lift and carry on the fully extended configuration while the dynamics of both the load and manipulator must be taken into account. The maximum load carrying capacity that can be achieved by a robotic manipulator during a given trajectory is limited by a number of factors. Probably, the most important factors are the actuator limitations, accuracy, amplitude of residual vibration and maximum stress. The dynamic stress of components is one of the most important dynamic parameters. If dynamic stress exceeds permissible stress, the flexible robot will be destroyed. On the other hand, residual vibration can effectively affect the manipulators performance and efficiency at the MADL for flexible link manipulators, in addition to two earlier constraints: actuator torque capacity and end-effector precision constraints.

Many approaches have been taken to the development of an accurate dynamic model for flexible manipulators [1-2]. Book has developed nonlinear equations of motion for flexible manipulator arms consisting of rotary joints that connect pairs of flexible links. The link deflection is assumed small, so that the link transformation can be composed of summations of assumed link shapes [3]. Meghdari carried out a general technique to model flexible components of manipulator arms based on Castigliano's theorem. The robotic arms flexibility properties are derived and represented by

1. *Robotic Research Laboratory, College of Mechanical Engineering, Iran University of Science and Technology, Tehran, P.O. Box 18846, Iran.*
*. *Corresponding author. E-mail: hkorayem@iust.ac.ir*

Received 9 April 2009; received in revised form 30 July 2009; accepted 19 September 2009

the matrix of compliance coefficients [4]. Damaran and Sharf have presented and classified the inertial and geometric nonlinearities that arise in the motion and constraint equations for multibody systems. They observed that for sufficiently fast maneuvers of the flexible links of manipulators, the linear beam theory approximation is completely inadequate [5]. Zhang carried out the dynamic modeling and simulation of two cooperating structurally flexible robotic manipulators [6].

Most of the researchers, however, assume small deformation and use a linear strain-displacement relationship [7-8]. When high speed, light weight, accuracy and large payload robots are considered, nonlinear elastic deformation in structures may have to be considered. Absy and Shabana show that the consideration of longitudinal displacement caused by bending would eliminate the third and higher order terms from the strain-energy expression, if the strain energy is written in terms of axial deformation. This leads to nonlinear inertia terms and a constant stiffness matrix [9]. Mayo et al. derived the dynamic equations of several flexible link mechanisms considering complete geometrical nonlinearity. Their proposed formulation considers the effect of geometric elastic nonlinearity on bending displacements without the need to use any axial vibration mode, so it is computationally very efficient [10]. Bakr presented a method for the dynamic analysis of geometrically nonlinear elastic robot manipulators. Robot arm elasticity is introduced using a finite element method that allows for gross arm rotations. Geometric elastic nonlinearities are introduced into the formulation by retaining the quadratic terms in the strain-displacement relationships [11]. Shaker and Ghosal considered the nonlinear modeling of planar, one- and two-link flexible manipulators with rotary joints using a finite element method. The equations of motion are derived, taking into account the nonlinear strain-displacement relationship, and two characteristic velocities, U_a and U_g, representing material and geometric properties, are used to nondimensionalize the equations of motion. The effect of variation of U_a and U_g on the dynamics of a planar flexible manipulator is brought out using numerical simulations [12]. Pratiher considered the non-linear vibration of a harmonically excited single link roller-supported flexible Cartesian manipulator with a payload. The governing equation of motion is developed using the extended Hamilton principle, which is reduced to a second-order temporal differential equation of motion by using a generalized Galerkin method [13]. Zohoor obtained the nonlinear dynamic model of a flying manipulator with two revolute joints and two highly flexible links using Hamilton's principle. In the issue of flying flexible-link manipulators, new terminologies, namely forward/inverse kinetics instead of forward/inverse kinematics, are suggested since determination of the position and orientation of the end-effector is coupled to the partial differential motion equations [14].

Wang and Ravani showed that the maximum allowable load of a fixed base manipulator on a given trajectory is primarily constrained by the joint actuator torque and its velocity characteristic [15]. Korayem and Ghariblu determined the maximum allowable load of wheeled mobile manipulators for a desired trajectory [16]. Yue computed the maximum payload of kinematically redundant manipulators using a finite element method for describing the dynamics of a system [17]. Korayem and Shokri developed an algorithm for finding the MADL of the 6-UPS Stewart platform manipulator [18]. Korayem and Heidari presented a general formula for finding the maximum allowable dynamic load of flexible link mobile manipulators. The main constraints used for the proposed algorithm are the actuator torque capacity and the limited error bound for the end-effector during motion on a given trajectory [19].

The dynamic stress of elastic mechanisms or flexible robots has been studied by a few researchers. Zhaocai studied the dynamic stress of the flexible beam element of planar flexible manipulators. Considering the effects of bending-shearing strain and tensile-compression strain, the dynamic stress of the links and its position are derived by using the Kineto-Elastodynamics theory and the Timoshenko beam theory [20]. Various approaches have previously been developed for reducing the residual vibration. Korayem et al. have considered the effect of payload on the residual vibration's amplitude. In order to apply the proposed constraint to the MADL calculation, they have defined an algorithm for the effect of payload on the residual vibration amplitude [21]. Abe proposed an optimal trajectory planning technique for suppressing residual vibrations in two-link rigid-flexible manipulators. In order to obtain an accurate mathematical model, the flexible link is modeled by taking the axial displacement and nonlinear curvature arising from large bending deformation into consideration [22].

In this paper, the equations of motion are derived, taking into account the nonlinear strain-displacement relationship using finite element method approaches. The strain energy is formulated in accordance with the slender beam theory and various non-linear terms are identified. The finite element method, which is able to consider the full nonlinear dynamic of a mobile manipulator, is applied to derive the kinematic and dynamic equations. Then, a method for determination of the maximum allowable dynamic load for a specific reference is explained, subject to the accuracy, actuator, maximum stress limitation and amplitude of residual vibration constraints. In order to verify the effectiveness of the presented algorithm, two simulation studies, considering a flexible two-link planar manipulator mounted on a mobile base, are presented and the results are discussed.

NONLINEAR STRAIN-DISPLACEMENT RELATIONSHIP

If the displacements are large enough, nonlinear strain-displacement relations have to be used. For in-plane bending of beams, only the normal strain, ε_{xx}, needs to be considered, and the full nonlinear strain-displacement relationship for ε_{xx} (assuming a 2-D problem) is given by:

$$\varepsilon_{xx} = \frac{\partial u_x^*}{\partial x} + \frac{1}{2}\left[\left(\frac{\partial u_x^*}{\partial x}\right)^2 + \left(\frac{\partial u_y^*}{\partial x}\right)^2\right]. \tag{1}$$

For small strain, $\left(\frac{\partial U_x^*}{\partial x}\right)^2$ can be ignored in comparison to $\frac{\partial u_x^*}{\partial x}$ and we have [23]:

$$\varepsilon_{xx} = \frac{\partial u_x^*}{\partial x} + \frac{1}{2}\left(\frac{\partial u_y^*}{\partial x}\right)^2,$$

$$\frac{\partial u_x^*}{\partial x} \gg \left(\frac{\partial u_x^*}{\partial x}\right)^2, \tag{2}$$

where the variables u_y^* and u_x^* denote the field-displacement variables defined over the entire domain. Furthermore, from the classical beam theory, we can write:

$$\varepsilon_{xx} = \frac{\partial u_x}{\partial x} - y\frac{\partial^2 u_y}{\partial x^2} + \frac{1}{2}\left(\frac{\partial u_y}{\partial x}\right)^2, \tag{3}$$

where y is measured from the neutral axis of the beam and u_x and u_y denote the longitudinal and transverse displacement, respectively, at $y = 0$. This is the nonlinear strain-displacement relationship that has been used in this paper for nonlinear modeling.

Assuming a linear stress-strain relationship, the potential energy can be obtained as:

$$U = \frac{E}{2}\int_v \varepsilon_{xx}^2 dV. \tag{4}$$

Expanding the above integral, and since y is measured from the neutral axis, all integrals of the form $\int ydA$ must vanish, then we get:

$$U = \frac{EA}{2}\int_0^l \left[\left(\frac{\partial u_x}{\partial x}\right)^2 + \left(\frac{\partial u_x}{\partial x}\right).\left(\frac{\partial u_y}{\partial x}\right)^2\right] dx$$
$$+ \frac{EI}{2}\int_0^l \left(\frac{\partial^2 u_y}{\partial x_{1j}^2}\right)^2 dx + \frac{EA}{2}\int_0^l \frac{1}{4}\left(\frac{\partial u_y}{\partial x}\right)^4 dx, \tag{5}$$

where E, A, I and l denote Young's modulus, the cross-sectional area, moment of inertia of the cross section and the length, respectively.

For the assumed nodal displacements and rotations, the displacement of any arbitrary point in the element can be expressed as:

$$\begin{Bmatrix} u_{xi} \\ u_{yi} \end{Bmatrix} = \begin{bmatrix} N_1 & 0 & 0 & N_4 & 0 & 0 \\ 0 & N_8 & N_9 & 0 & N_{11} & N_{12} \end{bmatrix} \{q_i\}^T, \tag{6}$$

where the shape functions, N_i, are given by $\left(\xi = \frac{x}{l}\right)$.

$$N_1 = 1 - \xi, \qquad N_4 = \xi,$$
$$N_8 = 1 - 3\xi^2 + 2\xi^3, \quad N_9 = (\xi - 2\xi^2 + \xi^3)l, \tag{7}$$
$$N_{11} = 3\xi^2 - 2\xi^3, \qquad N_{12} = (-\xi^2 + \xi^3)l.$$

The quantities u_{xi} and u_{yi} are the displacements of any arbitrary point of the ith element along the x-axis and y-axis, respectively. The vector of nodal degrees of freedom of the ith beam element (Figure 1) is given by:

$$\{q_i\} = \{u_{2i-1} \quad v_{2i-1} \quad \phi_{2i-1} \quad u_{2i} \quad v_{2i} \quad \phi_{2i}\}.$$

DYNAMIC MODEL OF FLEXIBLE MANIPULATOR

The overall approach involves treating each link of the manipulator as an assemblage of n_i elements of length, l_i. For each of these elements, the kinetic energy, T_{ij}, and potential energy, U_{ij}, are computed in terms of a selected system of n generalized variables $q = (q_1, q_2, \cdots, q_n)$ and their rate of change, $\dot{q}$. Dynamic equations for systems are derived through Lagrange equations:

$$\frac{d}{dt}\left(\frac{\partial \pounds}{\partial \dot{q}_k}\right) - \frac{\partial \pounds}{\partial q_k} = Q_k, \qquad k = 1, 2, \cdots, n. \tag{8}$$

The Lagrangian of link 1 is, as follows:

$$\pounds_1 = T_1 - U_1$$
$$= \frac{1}{2}\dot{q}_1^T M_1 \dot{q}_1 - m_1 g \begin{bmatrix} 0 & 1 \end{bmatrix} \vec{r}(x) - \frac{1}{2}\psi_1^T K_1 \psi_1, \tag{9}$$

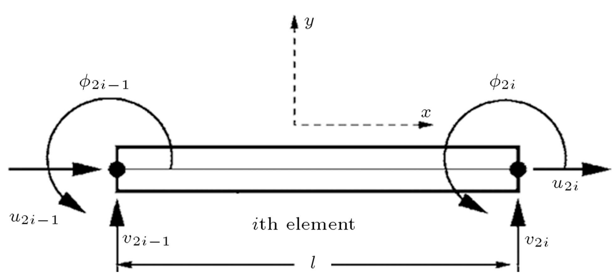

Figure 1. Planar beam element.

where:

$$q_1 = [\theta_1, \psi_1^T]^T,$$

and:

$$\psi_1 = [u_1, v_1, \phi_1, \cdots, u_{2n_1}, v_{2n_1}, \phi_{2n_1}]^T.$$

The Lagrangian of link 2 can be derived as:

$$\pounds_2 = T_2 - U_2$$

$$= \frac{1}{2}\dot{q}_2^T M_2 \dot{q}_2 - m_2 g \begin{bmatrix} 0 & 1 \end{bmatrix} \vec{r}(x) - \frac{1}{2}\psi_2^T K_2 \psi_2, \quad (10)$$

where:

$$q_2 = [\theta_1, u_{2n_1}, v_{2n_1}, \phi_{2n_1}, \theta_2, \psi_2^T]^T,$$

and:

$$\psi_2 = [p_1, w_1, \varphi_1, \cdots, p_{2n_2}, w_{2n_2}, \varphi_{2n_2}]^T.$$

The overall Lagrangian for a two-link flexible mobile manipulator with the base motion in a x direction can then be written as:

$$\pounds = \pounds_1(x_b, \theta_1, u_1, v_1, \phi_1, \cdots, u_{2n_1}, v_{2n_1}, \phi_{2n_1}) + \pounds_2(x_b, \theta_1, u_{2n_1}, v_{2n_1}, \phi_{2n_1}, \theta_2, p_1, w_1, \varphi_1, \cdots, p_{2n_2}, w_{2n_2}, \varphi_{2n_2}). \quad (11)$$

By applying Lagrange's equation and performing some algebraic manipulations, the compact form of the system's dynamic equations becomes [24]:

$$[M(q)]\{\ddot{q}\} + ([K_L] + [K_{NL}])\{q\} + h(q, \dot{q}) = \tau, \quad (12)$$

where $[M]$ is the system mass matrix, $[K_L]$ is the conventional stiffness matrix and $[K_{NL}]$ is the geometrically nonlinear stiffness matrix. $h(q, \dot{q})$ considers the contribution of other dynamic forces, such as centrifugal, Coriolis and gravity forces, while τ consists of input torques at the joints. In our approach, since each element of the link is assumed to have its own local coordinate system, for clamped boundary conditions, we have the constraints u_{2i-1}, v_{2i-1} and ϕ_{2i-1} to be zero of link 1. Also, the second link is constrained to have the constraints p_{2i-1}, w_{2i-1} and φ_{2i-1} to be zero. It must be noted that u_{2i-1}, v_{2i-1}, p_{2i-1}, w_{2i-1} and ϕ_{2i-1}, φ_{2i-1} are local displacements and rotation in the ith coordinate system.

MADL FORMULATION FOR A GIVEN TRAJECTORY

The Maximum Allowable Dynamic Load (MADL) that can be achieved by a manipulator during a given trajectory is limited by a number of factors. The most important ones are: the dynamic specification of the manipulator, the actuator limitations, accuracy, amplitude of residual vibration and maximum stress. A flexible manipulator can be considered to carry a maximum load when the path accuracy is maintained. This is highly critical when dealing with flexible link robots. The path accuracy must, therefore, be considered in MADL determination by imposing this constraint to the end-effector deflection, as well as to the actuator torque. Failing this, an excessive deviation may be caused due to an end-effector deflection for a given trajectory, even though the joint torque constraint is not violated. The dynamic stress of components is one of the most important dynamic parameters. If dynamic stress exceeds permissible stress, the flexible robot will be destroyed. On the other hand, residual vibration can effectively affect the manipulators performance and efficiency at the MADL for flexible link manipulators, in addition to two earlier constraints: actuator torque capacity and end-effector precision constraints. By considering constraints and adopting a logical computing method, the maximum load carrying capacity of a mobile manipulator for a given trajectory can be computed.

Formulation of Joint Actuator Torque Constraint

Based on the definition of typical torque-speed characteristics of DC motors, the joint actuator torque constant was formulated as follows [19]:

$$U_{\text{allow}}^{(+)} = c_1 - c_2\dot{q}, \qquad U_{\text{allow}}^{(-)} = -c_1 - c_2\dot{q}, \quad (13)$$

where $c_1 = \tau_s$, $c_2 = \tau_s/\omega_0$ and τ_s is the stall torque, ω_0 is the maximum no-load speed of the motor and $u_a^{(+)}$ and $u_a^{(-)}$ are the upper and lower bounds of the allowable torque. The left hand side of both equations above give the upper and lower allowable torques ($U_a^{(+)}$ and $U_a^{(-)}$) of any actuators. An experimental mass (m_e), less than the maximum estimated load, is then used in order to calculate τ_e for any ith point along the given trajectory. The allowable torque limits ($\tau_i^{(+)}$ and $\tau_i^{(-)}$) can then be calculated using the upper and lower allowable torques of the actuators and $(\tau_e)_i$ according to the following equations:

$$\tau_i^{(+)} = \left(U_a^{(+)}\right)_i - (\tau_e)_i,$$

$$\tau_i^{(-)} = \left(U_a^{(-)}\right)_i - (\tau_e)_i. \quad (14)$$

The maximum allowable torque of any joint $(\tau_a)_i$ can then be calculated as follows:

$$(\tau_a)_i = \max\left\{\tau_i^{(+)}, \tau_i^{(-)}\right\}. \quad (15)$$

In order to determine the maximum allowable load by considering the actuator constraint, it is essential to define a load coefficient $(c_a)_j$ for any point along the given trajectory as follows:

$$(c_a)_j = \min\left\{\frac{(\tau_a)_i}{\max(\tau_e) - \max(\tau_n)}\right\},$$

$$i = 1, 2, \cdots, n, \tag{16}$$

where τ_n represent the no-load torque. Physically, the load coefficient $(c_a)_j$ on the jth joint actuator describes the accessible torque for carrying the maximum load to the torque, which is applied for carrying the initial load.

Formulation of Accuracy Constraint

By considering the accuracy constraint, the path is discretized into m separate points. The deviation of the end-effector from a desired trajectory is then calculated for each point where $(\Delta_n)_j$ represents no-load deflection and $(\Delta_e)_j$ represents deflection under experimental load. The quantity and direction of deviation due to the experimental mass (m_e) for a selected point, j, along the given trajectory can be seen in Figure 2. A cubical boundary of radius R_p, as the end-effector's deflection constraint, can be used with the center of the cube positioned on the selected point on the given trajectory. $(\Delta_e)_j$ is a part of R_p that shows how much load can be carried without ignoring the accuracy constraint at point j. The difference between allowable deviation (R_p) and the amount of deviation due to experimental mass $(\Delta_e)_j$ can be considered as the remaining allowable deviation from the given trajectory that can be tolerated. As explained previously, there is a necessity to define a new load coefficient $(c_p)_j$ for each point along the given trajectory as follows:

$$(c_p)_j = \min\left\{\frac{R_p - (\Delta_e)_j}{\max(\Delta_e) - \max(\Delta_n)}\right\},$$

$$j = 1, 2, \cdots, m, \tag{17}$$

where Δ_n represents the no-load deviation of the end-effector from the given trajectory.

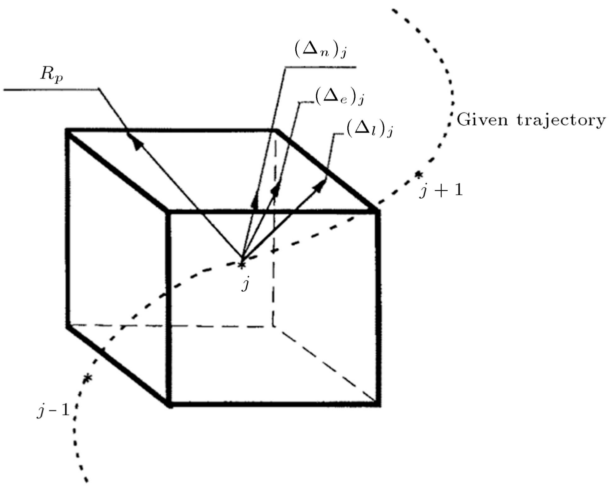

Figure 2. The cubical boundary on end-effector's deflection.

Formulation of Stress Constraint

Usually, longitudinal force, transverse force and bending moment are simultaneously exerted on the cross-section of links. Therefore, bending stress, tensile stress and shearing stress exist on the cross-section. Because the longer and thinner links are commonly used for flexible robots, the shearing stress is far lower than the bending stress and tensile stress. Therefore, the shearing stress used to be omitted by many researchers. To obtain the accurate dynamic stress, the effects of bending strain and tensile-compression strain are all taken into account. The bending stress, $\sigma_b(x,t)$, of the element can be expressed as:

$$\sigma_{\text{Bending}}(x,t) = E.\varepsilon_{xx}, \tag{18}$$

where x is the distance from the left end of the element to the given point; E is the elastic modulus and ε_{xx} is the full nonlinear strain. The tensile stress, $\sigma_p(x,t)$, of the element can be expressed as:

$$\sigma_{\text{Tension}} = \frac{E}{L}.(u_x^{2i} - u_x^{2i-1}). \tag{19}$$

Thus, the absolute value of the dynamic stress (normal stress) $\sigma(x,t)$ can be expressed as:

$$\sigma(x,t) = \frac{E}{L}\left|u_x^{2i}(t) - u_x^{2i-1}(t)\right| + E.\varepsilon_{xx}. \tag{20}$$

As the joint actuator torque constant, the stress constraint was formulated. The allowable stress limits ($\sigma_i^{(+)}$ and $\sigma_i^{(-)}$) can then be calculated using the upper and lower allowable stresses of the links and $(S_e)_j$, according to the following equations:

$$\sigma_i^{(+)} = \left(U_s^{(+)}\right)_i - (\sigma_e)_i,$$

$$\sigma_i^{(-)} = \left(U_s^{(-)}\right)_i - (\sigma_e)_i, \tag{21}$$

where $U_s^{(+)}$ and $U_s^{(-)}$ are the upper and lower bounds of the allowable stress. An experimental mass (m_e) less than the maximum estimated load, is then used in order to calculate σ_e for any ith point along the given trajectory. The maximum allowable stress of any joint $(\sigma_a)_j$ can then be calculated as follows:

$$(\sigma_a)_i = \max\left\{\sigma_i^{(+)}, \sigma_i^{(-)}\right\}. \tag{22}$$

In order to determine the maximum allowable load by considering the stress constraint, it is essential to define a load coefficient $(c_s)_j$ for any point along the given trajectory as follows:

$$(c_s)_j = \min\left\{\frac{(\sigma_a)_i}{\max(\sigma_e) - \max(\sigma_n)}\right\},$$

$$i = 1, 2, \cdots, n, \tag{23}$$

where σ_n represents the no-load stress.

Formulation of Residual Vibration Constraint

Residual vibrations start from time t_f from which the main path is tracked and there are some extra vibrations around the goal point as a result of flexibility in the system. The flexible robot will freely oscillate with the excitation of the final velocity of the end-effector. In previous works, by assuming small and slow deformation about the final configuration, the centrifugal and Coriolis forces, which increased non-linearity effects, were neglected. By considering these assumptions, the equations of motion in flexible robots can be linearized for final time. In other words, the high order terms, such as q_f^2, $\dot{q}_f^2$, q_f, $\dot{q}_f$, $\dot{\theta}$, $\ddot{\theta}$, etc., can be ignored in the equations of motion when the amplitude and velocity can be assumed small enough. These assumptions are true when the residual vibrations about the final configuration have small amplitude and low frequency. However, these assumptions will be violated in a wide variety of practical circumstances. In this paper, all the above mentioned assumptions are released and the entire non-linear terms are taken into account. In a wide variety of applications, it is expected that the amplitude of the residual vibration will be less than a definite value. Because of the presence of the elasticity in links, after stopping the robot, some redundant vibrations will start at the end effector.

Motion equations should be solved in two steps: First, for $0 \leq t \leq t_f$, the main path of which the robot is tracking and then for $t > t_f$, for the residual vibration. After solving these equations numerically, the position of the end-effector is obtained, which is expressed by:

$$\begin{aligned} r_{fx} = x_b &+ (L_1 - u_{2n_1+1})\cos\theta_{1f} \\ &+ (L_2 + u_{2n_2+1})\cos(\theta_{1f} + \theta_{2f} + u_{2n_1+3}) \\ &- u_{2n_2+2}\sin(\theta_{1f} + \theta_{2f} + u_{2n_1+3}) \\ &- u_{2n_1+2}\sin\theta_{1f}, \end{aligned}$$

$$\begin{aligned} r_{fy} = y_b &+ (L_1 - u_{2n_1+1})\sin\theta_{1f} \\ &+ (L_2 + u_{2n_2+1})\sin(\theta_{1f} + \theta_{2f} + u_{2n_1+3}) \\ &+ u_{2n_2+2}\cos(\theta_{1f} + \theta_{2f} + u_{2n_1+3}) \\ &+ u_{2n_1+2}\cos\theta_{1f}. \end{aligned} \tag{24}$$

The difference between the position of the goal point and the obtained path from a flexible robot can be found as follows:

$$e_x = r_{fx} - x_f, \qquad e_y = r_{fy} - y_f, \qquad t > t_f, \tag{25}$$

where x_f and y_f represent the position of the goal point. Finally, the absolute value of the position error can be defined as:

$$P_e = \sqrt{e_x^2 + e_y^2}. \tag{26}$$

The amount of these vibrations can be used as a new constraint in determining the MADL. Since there is not an explicit relation between the payload and the amplitude of residual vibration, a relation has been inferred through some simulations.

Figure 3 shows the residual vibration of the end effector around the goal point. In this figure, R_{rv} is the desired accuracy for residual vibration, R_e and R_{nl} are the amounts of maximum amplitude of residual vibration with and without the presence of the payload, respectively. Two circles are drawn in such ways that surround the vibration considering the goal point as their centre. The radius of this circle can be used as a criterion for the residual vibration's magnitude which

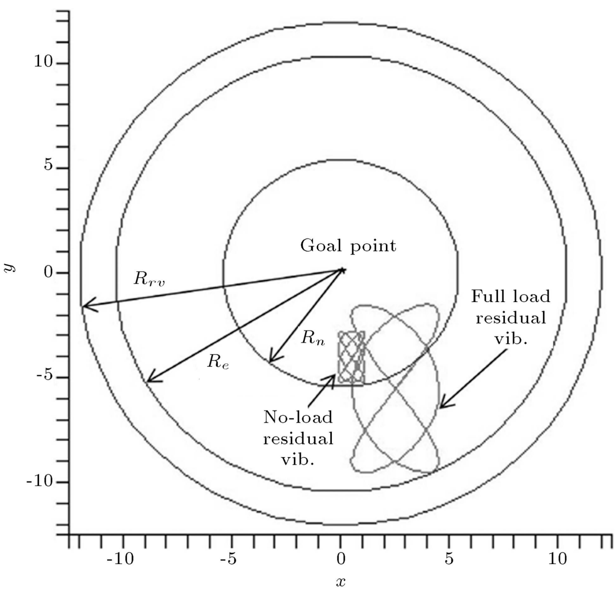

Figure 3. Maximum residual vibration of robot with and without considering the payload.

is called the Radius of Residual Vibration (RRV) in this article.

In order to ensure that all constraints are satisfied for all discretized points along the given trajectory, a general load coefficient, c, can be defined as follows:

$$c = \min\{(c_p)_j, (c_a)_j, (c_S)_j, (c_v)_j\},$$

$$j = 1, 2, \cdots, m. \tag{27}$$

As a result, the maximum allowable mass, m_{load}, can be calculated as follows:

$$m_{\text{load}} = cm_e. \tag{28}$$

SIMULATION

A simulation study has been carried out to investigate further the validity and effectiveness of the geometrically nonlinear flexible link and compute the MADL of a given trajectory. In order to initially check the validity of the dynamic equations, the response of the system with a very large elastic constant to an initial condition corresponding to $\theta_1 = -90°$ and $\theta_2 = 5°$ (Figure 4) has been simulated.

The parameter values of the model used in these simulation studies were $L_1 = L_2 = 1$ m, $I_1 = I_2 = 5 \times 10^{-9}$ m^4, $E = E = 2 \times 10$ N/m and $m_1 = m_2 = 5$ kg/m. As shown in Figures 5 to 7, the response of the system was in agreement with the harmonic motion of an elastic two-link robot hanging freely under gravity.

Several additional simulations of the system are performed. One is a classical example for geometrically

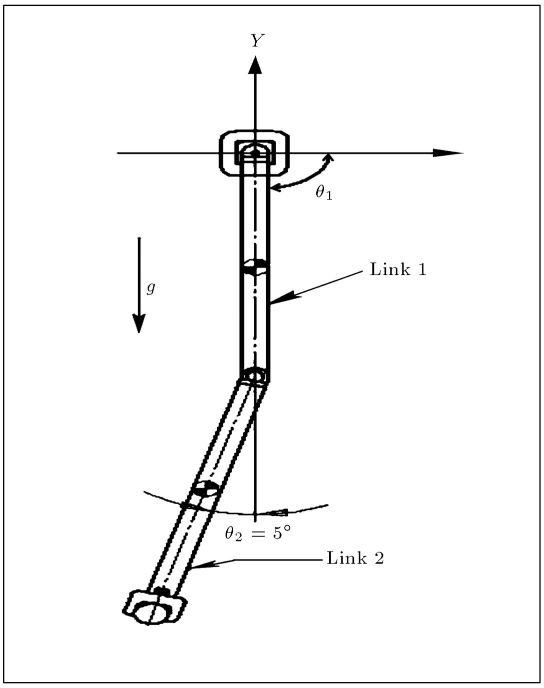

Figure 4. Initial condition for the model validity.

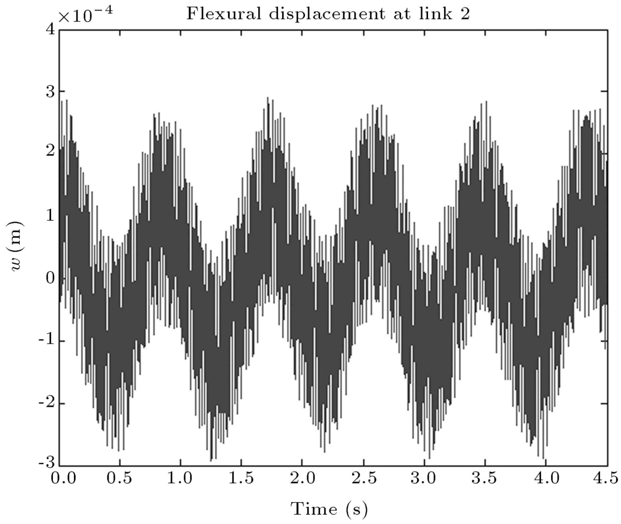

Figure 5. Lateral deflection at the tip of link 2.

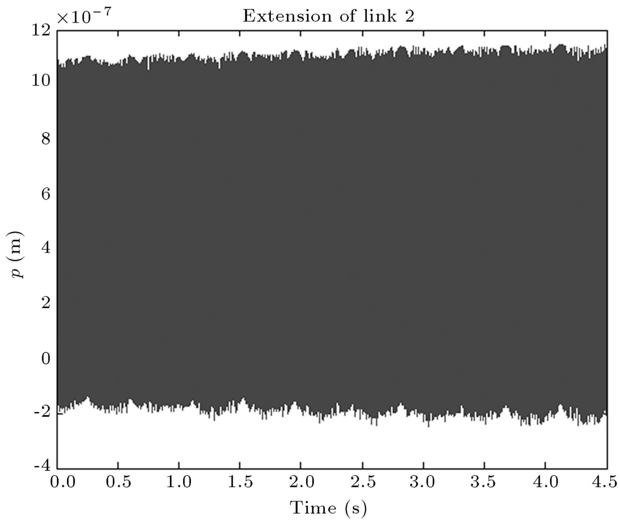

Figure 6. Axial deflection at the tip of link 2.

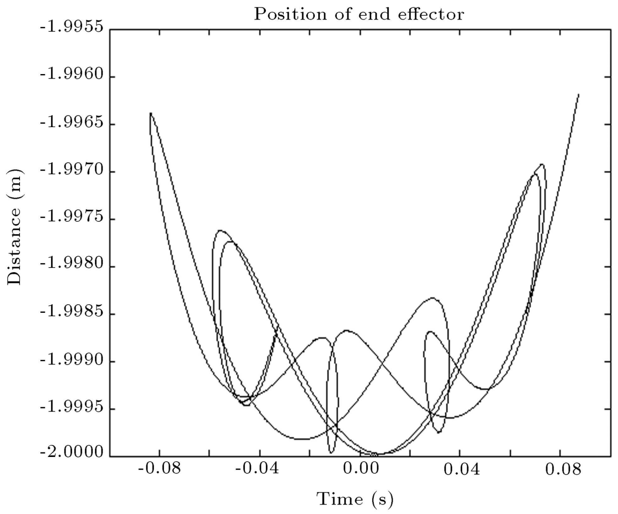

Figure 7. Endpoint trajectory viewed in global coordinate system.

elastic nonlinear formulations to illustrate the performance of the simulation and the effect of the geometric nonlinearity. In the second test, a robot manipulator with elastic links is considered. The end-effector and its load must track a straight line with a predefined speed. In the third test, MADL is found for a flexible robot manipulator in which the end-effector must move along a circular path. In the last two cases, the mobile base of the manipulator moves along a straight line at a constant speed.

1R Planar Rotating Flexible Manipulator

In this section, the dynamic characteristics of the rotating flexible manipulator are studied through numerical simulations (Figure 8), for the computational efficiency of geometric nonlinearity at high speed is comparable to that of a linear formulation. The properties of the flexible manipulator are the same as those in [10], and are given as follows:

The length: $L = 8$ m;

The cross section area: $A = 7.3 \times 10^{-5}$ m^2;

The second moment of area: $I = 8.218 \times 10^{-9}$ m^4;

The mass density: $\rho = 2.7667 \times 10^3$ kg/m^2;

The Young's modulus of material: $E = 68.95$ GPa.

The rotating flexible manipulator spun-up according to a motion law is defined by:

$$\theta(t) = \left(\frac{\omega_s}{T_s}\right)\left[\left(\frac{t^2}{2}\right) + \left(\frac{T_s}{2\pi}\right)^2\left(\cos\left(\frac{2\pi t}{T_s}\right) - 1\right)\right], \tag{29}$$

where ω_s and T_s are the rating angular velocity and start-up time, respectively. In this simulation, $T_s = 15$ s and the rotation speed, ω_s, is varied from 0.1 ras/s to 2.5 rad/s.

Figures 9 and 10 show the deflection obtained at an angular velocity, ω_s, of 1 and 2.5 rad/s, respectively. As can be seen, elastic displacements are small at a small angular velocity so both the linear

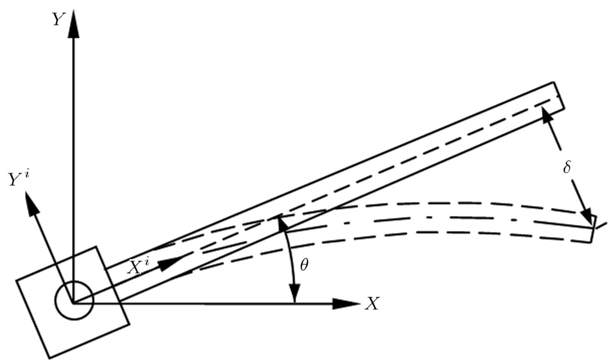

Figure 8. $1R$ planar rotating flexible manipulator.

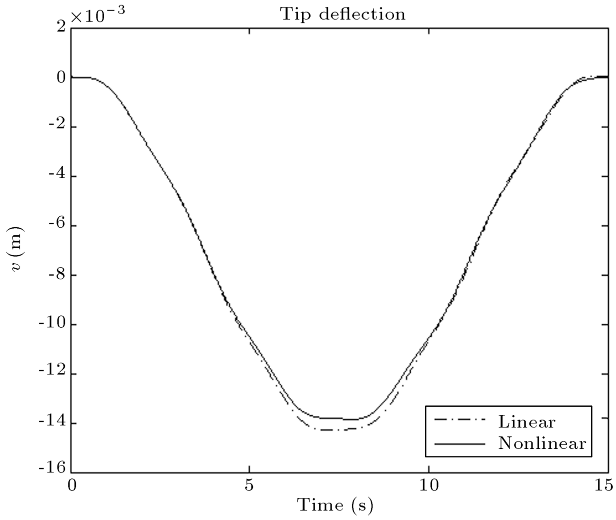

Figure 9. Deflection on the link end with $\omega_s = 0.1$ rad/s.

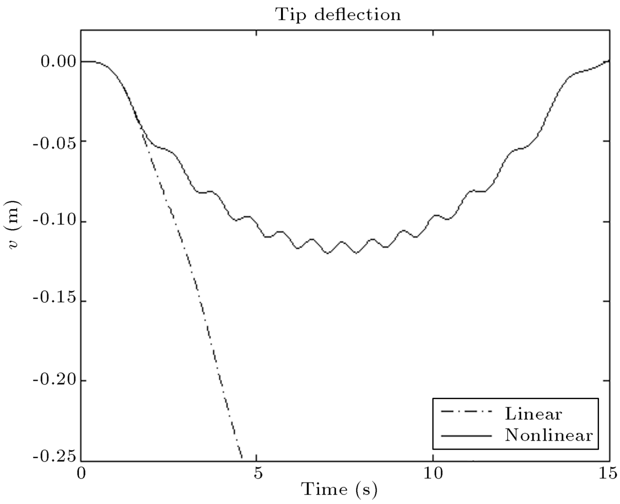

Figure 10. Deflection on the beam end with $\omega_s = 2.5$ rad/s.

and the nonlinear formulation lead to the same solution (Figure 9). As shown in Figure 10, when the angular velocity is raised to 2.5 rad/s, the results provided by the simulation, not including the effects of geometric elastic nonlinearity, are divergent and inconsistent with the actual physical response. This is the result of an increase in the rotation speed increasing both centrifugal axial forces and the displacement amplitude through deflection of the link.

MADL of a Flexible Mobile Manipulator with a Linear Path

This simulation study is performed to investigate the efficiency of the procedure presented in Figure 11 for computing the maximum allowable load of a mobile manipulator. All required parameters are given in Table 1. As mentioned earlier, the path of the end-

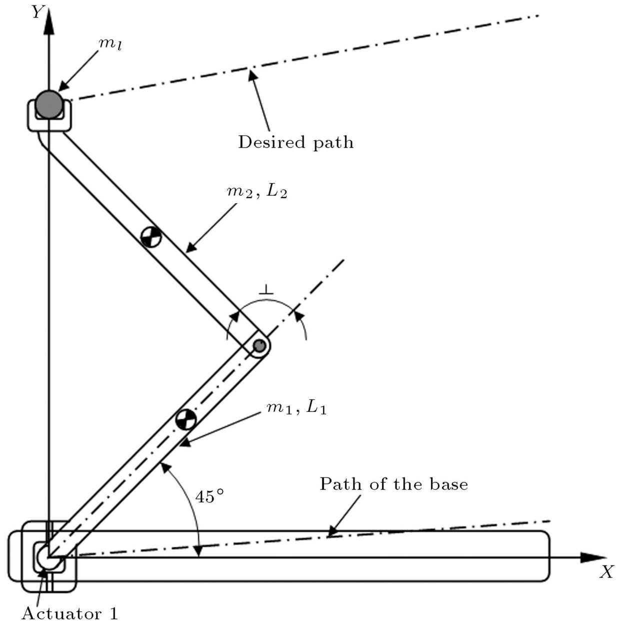

Figure 11. Schematic of robot and the desired path of end-effector.

Table 1. Simulation of parameters.

Parameter	Value	Unit
Length of links	$L_1 = L_2 = 2.5$	m
Mass	$m_1 = m_2 = 5$	kg
Cross section area	$A_1 = A_2 = 3 \times 10^{-4}$	m^2
Moment of inertia	$I_1 = I_2 = 5 \times 10^{-8}$	m^4
Young's modulus of material	$E_1 = E_2 = 4.5 \times 10^{10}$	N/m^2

effector and its payload is linear, which starts from point $x_1 = 0$ and $y_1 = 3.5$ m and ends at a point with coordinate $x_2 = 1.72$ m and $y_2 = 4.4$ m.

The velocity profile of the end-effector is as below:

$$\begin{cases} v = at & 0 \leq t \leq T/4 \\ v = v_{\max} & T/4 \leq t \leq 3T/4 \\ v = -at & 3T/4 \leq t \leq T \end{cases} \tag{30}$$

A linear path is planned for the vehicle, which starts from the origin and ends at $x_{b2} = 0.99$ m and $y_{b2} = 0.26$ m, with the velocity of $V_b = 0.2t$. The obtained path of the end-effector, considering link flexibility is shown in Figure 12 in comparison with the desired path. Also, the joint angles of rigid and flexible link states are shown in Figures 13 and 14. The corresponding applied torques to the manipulator actuators are shown in Figures 15 and 16.

Links can be regarded as cantilevers. Thus, the maximal dynamic stress should occur close to the joints. The numerical simulation results show that the maximal dynamic stresses of links change significantly with the load. As shown in Figures 17 and 18, the

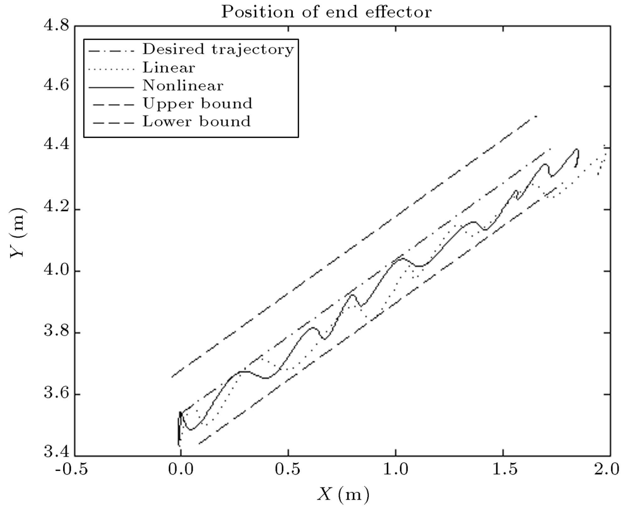

Figure 12. The desired and the actual load path.

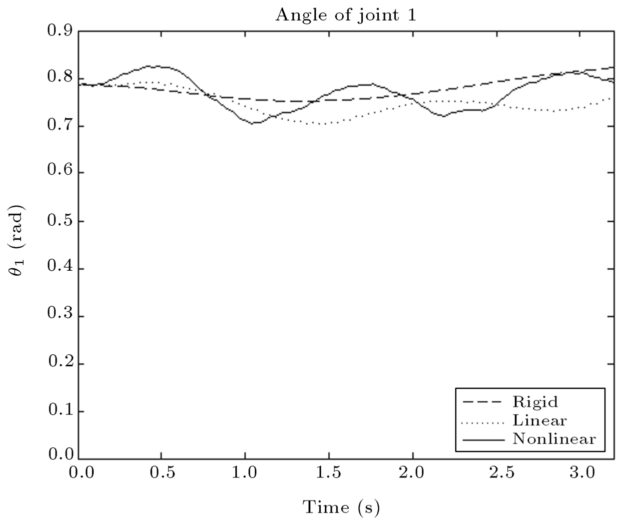

Figure 13. Joint responses of θ_1 for rigid and flexible links.

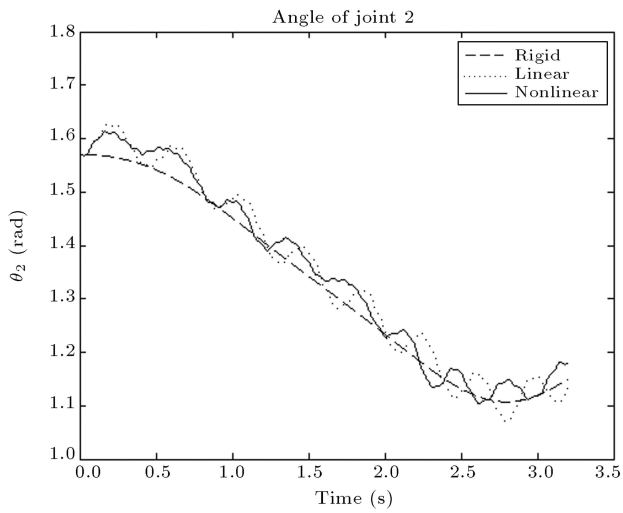

Figure 14. Angular positions of θ_2 for rigid and flexible links.

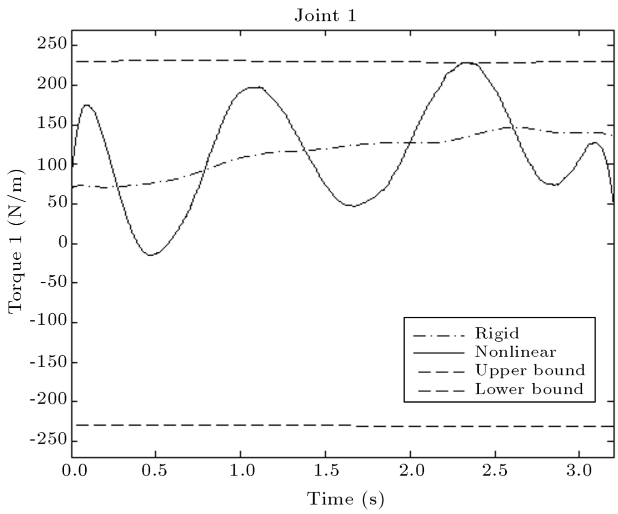

Figure 15. Actuator torque at the first joint against torque bounds.

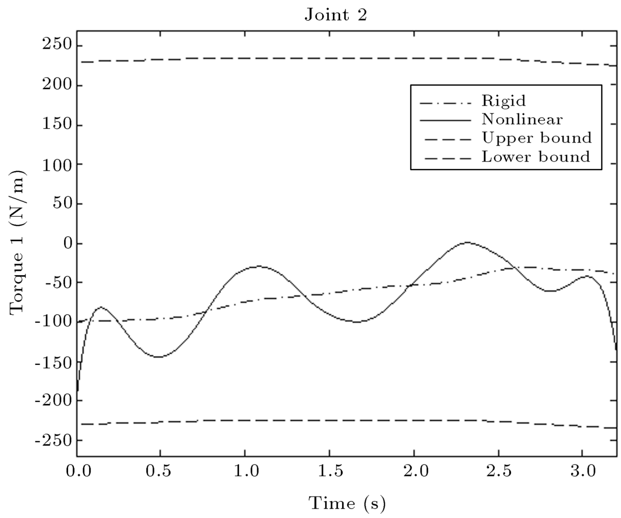

Figure 16. Actuator torque at the second joint.

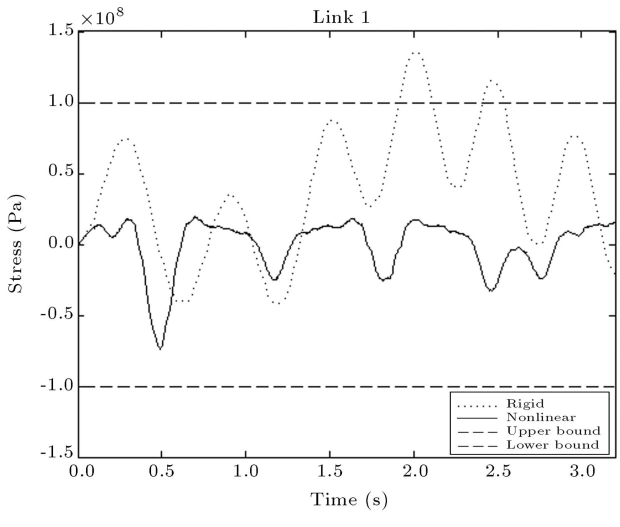

Figure 17. Maximal dynamic stress of flexible link 1 against stress bounds.

maximal dynamic stress values fluctuate frequently and arise to the admissible stress with maximum load.

The relation between the magnitude of residual vibration and the amount of payload is concluded. As can be seen, the flexibility of the link and adding the payload will non-linearily increase the amplitude of the residual vibrations. The variation trend of RRV, with respect to payload mass for a flexible link manipulator, is shown in Figure 19. This non-uniform increasing trend of RRV is because of displacement and velocity errors at the final time. Depending on the initial conditions, the magnitude of the residual vibration's amplitude may vary. With these descriptions, to estimate the residual vibration amplitude in terms of the payload value, a tangent line to the maximum value of RRV can be considered as shown in Figure 19. This line can be used for considering the residual

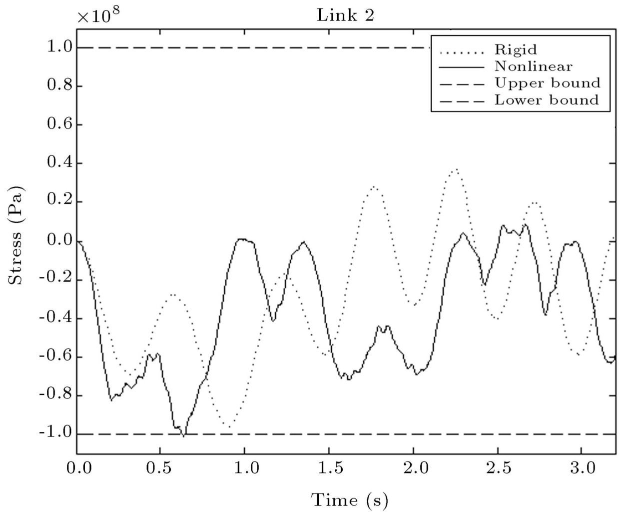

Figure 18. Maximal dynamic stress of flexible link 2 during the linear path.

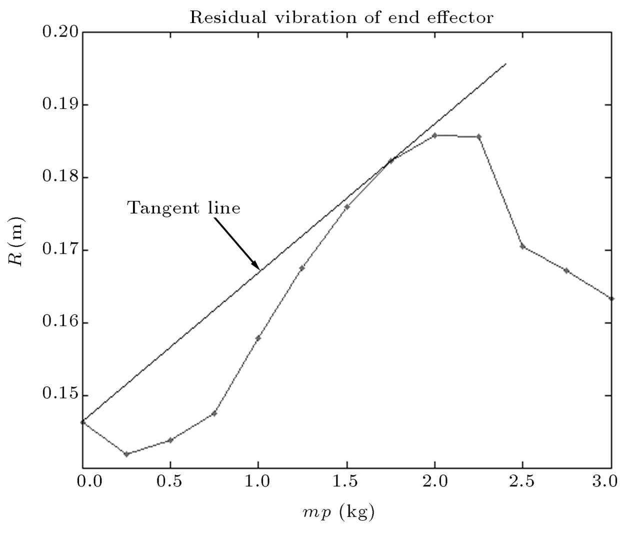

Figure 19. Maximum residual vibration versus payloads in the linear path.

vibration as a constraint in computing the maximum payload.

Now, the MADL of the robot of the previous section can be computed. The permissible error bound for the end-effector motion around the desired path is $R_p = 6$ cm, and at the end point is $R_{rv} = 16.5$ cm. Both actuators of the robot are considered to be the same, with $T_s = 230$ N.m and $\omega_{n1} = 10$ rad/s and allowable stresses of the links are considered to be the same with $U_s = 100$ MPa. The MADL, by imposing all constraints, are found and given in Table 2. Therefore, the maximum allowable dynamic load of the robot, considering all constraints, is calculated to be 0.91 kg for the given linear path.

MADL of a Flexible Mobile Manipulator with a Circular Path

In this simulation, the computation of the MADL for a two-link planar manipulator mounted on an XY table (Figure 20) is presented. The link parameters and inertia properties of the manipulator were given in Table 3. In the inertial reference frame, the XY table is capable of moving 1000 mm along the X-axis. Base velocity is $V_x = 0.1t$. Also, it is assumed that the load must move along a circular path. The centre of the circular path coordinates with radius $r = 50$ cm is at $x_c = 1$ m and $y_c = 1$ m with its origin at the lower-left corner of the XY table (Figure 21).

The obtained path which is tracked by the flexible robot manipulator is compared with the desired path in Figure 21. In this case, the permissible error bound for the end-effector motion around the desired path is $R_p = 6$ cm, and at the end point is $R_{rv} = 3$ cm.

Both actuators of the robot and allowable stresses are considered to be the same with $T_s = 170$ N.m, $\omega_{nl} = 5$ rad/s and $U_s = 100$ MPa, respectively. The corresponding applied torques to each actuator are shown in Figures 22 and 23. The maximal dynamic stresses are shown in Figures 24 and 25 and the variation trend of RRV with respect to payload mass for the flexible link manipulator with the circular path is shown in Figure 26. The MADL, by imposing imposing all constraints, is found and given in Table 4. Therefore, the maximum allowable dynamic load of the

Table 2. The MADL of robot with all constraints.

Constraint	MADL
Accuracy	1.1 kg
Actuator torque	2.52 kg
Maximum stress	5.62 kg
Accuracy-actuator torque	1.1 kg
Accuracy-residual vibration	0.91 kg
All	0.91 kg

Table 3. Parameters of two-link planar flexible manipulator.

Parameter	Value	Unit
Length of links	$L_1 = L_2 = 1.2$	m
Mass	$m_1 = M_2 = 2.4$	kg
Cross section area	$A_1 = A_2 = 3 \times 10^{-4}$	m^2
Moment of inertia	$I_1 = I_2 = 5 \times 10^{-8}$	m^4
Young's modulus of material	$E_1 = E_2 = 4.5 \times 10^{10}$	N/m^2

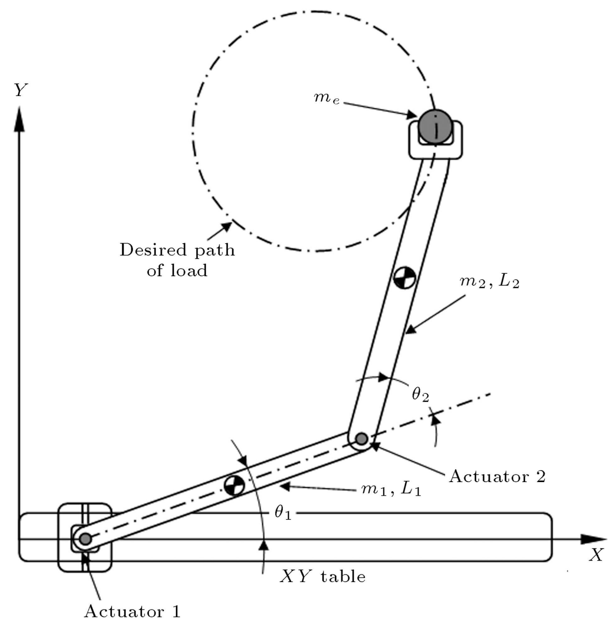

Figure 20. Schematic of flexible link planar manipulator with the circular path.

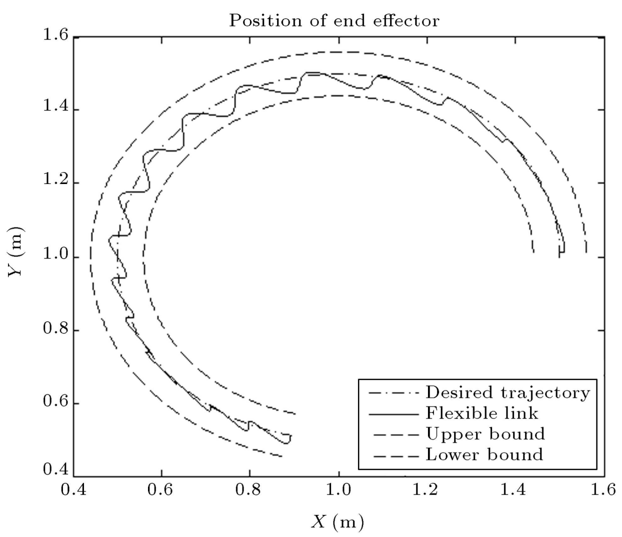

Figure 21. Desired and actual trajectory in the circular path.

robot considering all constraints is found to be 1.2 kg for the given trajectory.

The results depicted the importance of all constraints. According to accuracy and tracking, they show which one would be the main one. The simulation results indicate that the main reason for manipulator deviation is its major link's flexibility.

CONCLUSIONS

The main objective of this study was formulating and determining the Maximum Allowable Dynamic Load (MADL) for geometrically nonlinear flexible-link manipulators with a pre-defined trajectory, using the finite element method. A complete dynamic model is considered to characterize the motion of a compliant link capable of large deflection. The MADL was

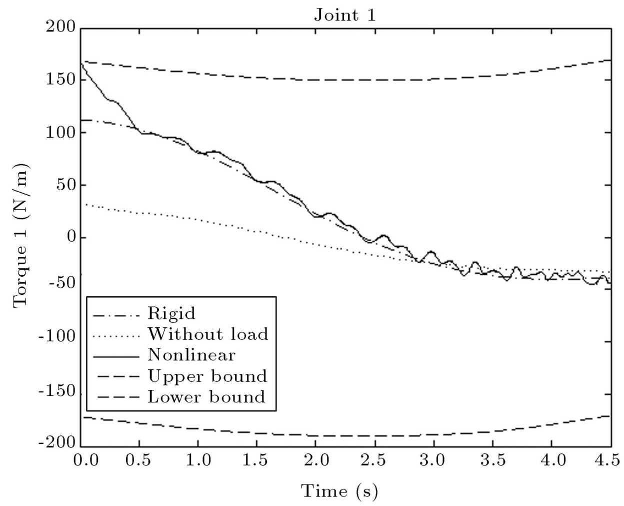

Figure 22. Variation of first joint torque with time within upper and lower acceptable boundaries.

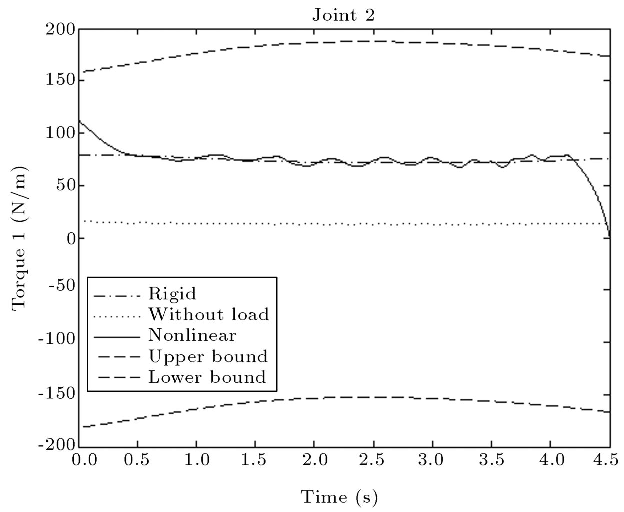

Figure 23. Applied torques of the second motor.

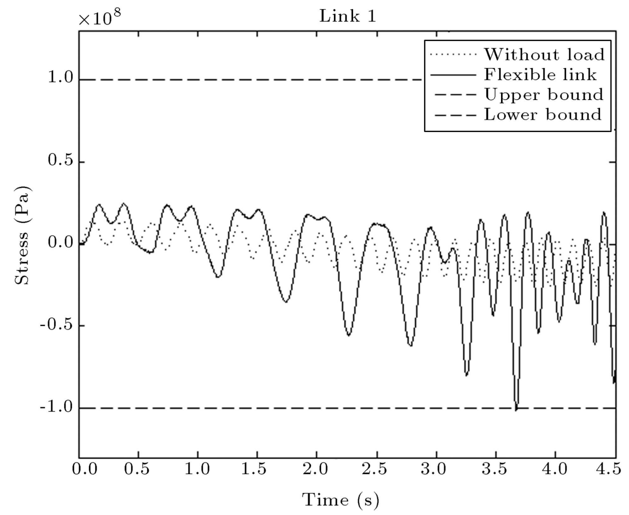

Figure 24. Maximum dynamic stress of flexible link 1 during the circular path.

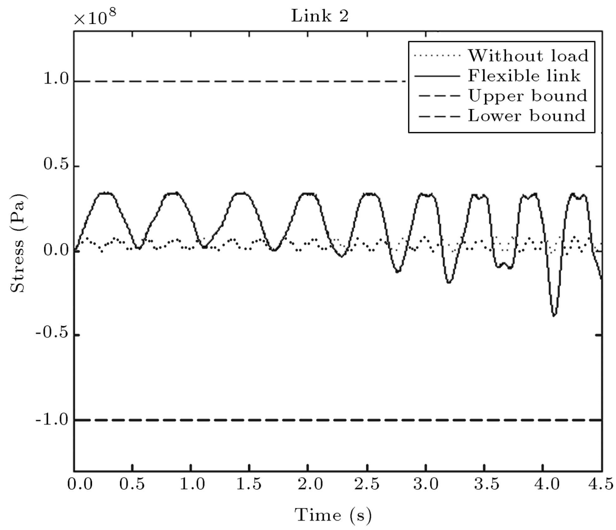

Figure 25. Maximal dynamic stress of flexible link 2 during the circular path.

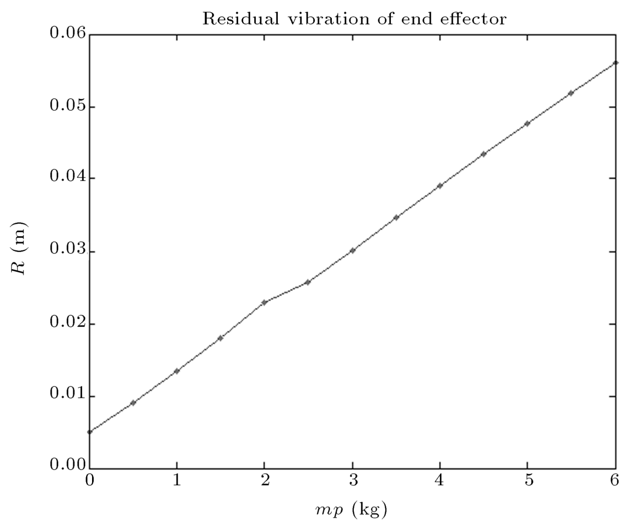

Figure 26. Radius of residual vibration versus payloads.

Table 4. Maximum allowable dynamic load in circular path.

Constraint	MADL
Accuracy	1.2 kg
Actuator torque	5.5 kg
Maximum stress	9.05 kg
Accuracy-actuator torque	1.2 kg
Accuracy-residual vibration	1.2 kg
All	1.2 kg

achieved by imposing actuator torque capacity, end effector accuracy, maximum stress and residual vibration constraints to the problem formulation. In simulation studies, a two-link planar manipulator mounted on a mobile base was considered for carrying a load in two-test cases. Numerical results obtained indicate that the inclusion of geometric elastic nonlinearities in the mathematical model leads to the development of a new geometrically nonlinear stiffness matrix whose neglect will affect the overall behavior of the robot. The results of the case study show that the allowable load is variable along the given trajectory. In addition, the formulation is more stable and efficient than most alternatives and has the added advantage of being able to calculate residual vibration and a new effective constraint, as "the dynamic stress constraint of links". Therefore, the permissible error bound for constraints in large deformation is sensitive in calculating the MADL.

NOMENCLATURE

θ_1, θ_2	angular displacements of joints 1 & 2
L_1, L_2	total lengths of links 1 and 2
m_1, m_2	total mass of links 1 and 2
I_1, I_2	moment of inertia of links 1 and 2
A_1, A_2	cross section of links 1 and 2
E_1, E_2	Young's modulus of links 1 and 2
u_{2i}	axial displacement at common junction of elements 'i' and '$i+1$' of link 1
v_{2i}	flexural displacement at common junction of elements 'i' and '$i+1$' of link 1
ϕ_{2i}	flexural slope at common junction of elements 'i' and '$i+1$' of link 1
n_1, n_2	number of elements of links 1 and 2
q_i	generalized coordinates
M_1, M_2	generalized inertia matrices of links 1 and 2
K_1, K_2	stiffness matrices of links 1 and 2
$r(x)$	vector from the origin to a point on element
r_{fx}, r_{fy}	the position of the goal point from flexible robot
p_{2i}	axial displacement at common junction of elements 'i' and '$i+1$' of link 2
w_{2i}	flexural displacement at common junction of elements 'i' and '$i+1$' of link 2
φ_{2i}	flexural slope at common junction of elements 'i' and '$i+1$' of link 2

REFERENCES

1. Al-Bedoor, B.O. and Hamdan, M.N. "Geometrically non-linear dynamic model of a rotating flexible arm", *Journal of Sound and Vibration*, **240**(1), pp. 59-72 (2001).
2. Liu, J.Y. and Hong, J.Z. "Geometric stiffening of flexible link system with large overall motion", *Computers and Structures*, **81**, pp. 2829-2841 (2003).
3. Book, W.J. "Recursive Lagrangian dynamics of flexible manipulator arms", *Int. J. Robotics Res.*, **3**(3), pp. 87-101 (1984).
4. Meghdari, A. "A variational approach for modeling flexibility effects in manipulator arms", *Robotica*, **9**, pp. 213-217 (1991).
5. Damaren, C. and Sharf, L. "Simulation of flexible-link manipulators with inertia and geometric nonlinearities", *ASME J. Dyn. Syst., Meas., Control*, **117**, pp. 74-87 (1995).
6. Zhang, C.X. and Yu, Y.Q. "Dynamic analysis of planar cooperative manipulators with link flexibility", *ASME J. of Dyn. Sys. and Control*, **126**, pp. 442-448 (2004).
7. Book, W.J. "Modeling, design, and control of flexible manipulator arms: a tutorial review", *Proc. of the IEEE Conf. on Decision and Control*, pp. 500-506 (1990).
8. Meghdari, A. and Fahimi, F. "On the first-order decoupling of dynamical equations of motion for elastic multibody systems as applied to a two-link flexible manipulator", *Multibody System Dynamics*, **5**, pp. 1-20 (2001).
9. Absy, H.E.L. and Shabana, A.A. "Geometric stiffness and stability of rigid body modes", *J. Sound Vib.*, **207**(4), pp. 465-496 (1997).
10. Mayo, J. and Dominguez, J. "A finite element geometrically nonlinear dynamic formulation of flexible multibody systems using a new displacements representation", *Vibration and Acoustics, ASME*, **119**, pp. 573-581 (1997).
11. Bakr, E.M. "Dynamic analysis of geometrically nonlinear robot manipulators", *Nonlinear Dynamics*, **11**, pp. 329-346 (1996).
12. Shaker, M.C. and Ghosal, A. "Nonlinear modeling of flexible manipulators using non-dimensional variables", *ASME, J. of Computer and Nonlinear Dyn.*, **1**, pp. 123-134 (2006).

13. Pratiher, B. and Dwivedy, S.K. "Non-linear dynamics of a flexible single link Cartesian manipulator", *Int. J. of Non-Linear Mechanics*, **42**, pp. 1062-1073 (2007).

14. Zohoor, H. and Khorsandijou, S.A.M. "Dynamic model of a flying manipulator with two highly flexible links", *Applied Mathematical Modelling*, **32**, pp. 2117-2132 (2008).

15. Wang, L.T. and Ravani, B. "Dynamic load carrying capacity of mechanical manipulators - Part I: Problem formulation", *ASME, J. of Dyn. Sys., Meas. & Cont.*, **110**, pp. 46-52 (1988).

16. Korayem, M.H. and Ghariblu, H. "Maximum allowable load on wheeled mobile manipulators imposing redundancy constraints", *J. of Rob. & Auto. Sys.*, **44**(2), pp. 151-159 (2003).

17. Yue, S. and Tso, S.K. "Maximum dynamic payload trajectory for flexible robot manipulators with kinematic redundancy", *Mech. Mach. Theory*, **36**, pp. 785-800 (2001).

18. Korayem, M.H. and Shokri, M. "Maximum dynamic load carrying capacity of a 6 ups-stewart platform manipulator", *Scientia Iranica*, **15**(1), pp. 131-143 (2008).

19. Korayem, M.H. and Heidari, A. "Maximum allowable dynamic load of flexible mobile manipulators using finite element approach", *Adv. Manuf. & Tech.*, **36**, pp. 606-617 (2007).

20. Zhaocai, D. "Analysis of dynamic stress and fatigue property of flexible robot", *Proc. of IEEE Int. Conf. on Rob. and Bio*, pp. 1351-1355 (2006).

21. Korayem, M.H., Nikoobin, A. and Heidari, A. "The effect of payload variation on the residual vibration of flexible manipulators at the end of the given path", *Scientica Iranica, Transaction B*, **16**(4), pp. 332-343 (2009).

22. Abe, A. "Trajectory planning for residual vibration suppression of a two-link rigid-flexible manipulator considering large deformation", *Mech. Mach. Theory*, **44**, pp. 1627-1639 (2009).

23. Crisfield, M.A., *Nonlinear Finite Element Analysis of Solids and Structures*, John Wiley & Sons, England (2001).

24. Robinett III, R.D., Feddema, J., Eisler, G.R., Dohrmann, C., Parker, G.G., Wilson, D.G. and Stokes, D., *Flexible Robot Dynamics and Controls*, IFSR International Series on Systems Science and Engineering, **19**, New York, Plenum Publishers (2002).